JMATPRO	Journal of Advanced Materials and Processing 10 (2): 29-38, Spring 2022 http://jmatpro.iaun.iau.ir 20.1001.1.2322388.2022.10.2.4.9

Research Paper

Influence of Withdrawal Rate on As-Cast Microstructure and Stress-Rupture Life of Directionally Solidified Rene80 Superalloy

Sobhan Rajabinejad, Masumeh Seifollahi*, Seyed Mahdi Abbasi, Seyed Mahdi Ghazi mirsaeed

Faculty of Materials and Manufacturing Technologies, Malek Ashtar University of Technology, Tehran, Iran.

ARTICLE INFO

Article history:

Received 11 January 2022
Accepted 26 March 2022
Available online 1 April 2022

Keywords:
Rene80
DS superaloy
Withdrawal rate
Dendritic structure
Microporosity
Stress-rupture

ABSTRACT

The purpose of this study is to investigate the effects of withdrawal rate on the dendrite microstructure and its formation mechanism, the porosity, and the interaction between them in Rene 80 superalloy. So, Rene 80 Ni-base superalloy was directionally solidified on a laboratory scale using the Bridgman method. The cylindrical rods were grown at withdrawal rates of 2, 4, 6, 8, and 10 $mm.min^{-1}$. Dendritic structure and solidification microporosities were evaluated in transverse and longitude sections. The results showed that when the withdrawal rate was increased, the primary and secondary dendritic arm spacing decreased. With an increasing withdrawal rate, which causes to decrease in the dendritic arms spacing, the volume fraction of inter-dendritic gamma prime was first decreased until the rate of 6 $mm.min^{-1}$, and after that, its volume fraction increased. This structure results from peritectic and eutectic transformations with checkerboard-like and fan-like morphology, respectively. Moreover, the volume fraction of microporosities was minimal at the rate of 6 $mm.min^{-1}$, while their average size decreased from 13.2 to 8.7 µm. The specimens were given a two-stage heat treatment followed by a stress rupture test at 191 MPa and 980˚C. It was shown that at R=6 $mm.min^{-1}$, directionally solidified rods with a less solidification microporosity and well-orientated dendritic structure give higher rupture life of 25.43 hrs.

Citation: Rajabinejad, S.; Seifollahi, M.; Abbasi, S.M.; Ghazi mirsaeed, S.M. (2022). Influence of Withdrawal Rate on As-Cast Microstructure and Stress-Rupture Life of Directionally Solidified Rene80 Superalloy, Journal of Advanced Materials and Processing, 10 (2), 29-38. Dor: 20.1001.1.2322388.2022.10.2.4.9

* **Corresponding Author**
E-mail Address: m_seifollahi@alumni.iust.ac.ir

1. Introduction

The high-temperature properties of nickel-base superalloys lead to their extensive application in jet engines and gas turbines [1]. Due to a good combination of tensile and stress rupture strength, long-term thermal stability, thermal fatigue, and hot corrosion resistance, the cast Rene80 Ni-base superalloy has been used extensively as the first and second stages of jet engine blades [2-6]. Work by Ohtomo et al. [3] demonstrated that tensile properties and rupture life of Rene 80 superalloy could be improved 10-15% and 2-3 times, respectively by directional solidification process. During the process of solidification, the porosities could form inevitably, which are difficult to be compensated by the interdendritic liquid flow. Undoubtedly, these porosities seriously deteriorate the high-temperature mechanical, especially fatigue properties of turbine blades [7-9]. Microporosities are classified into four groups: gas, solidification (S-type), heat treatment (H-type), and deformation (D-type). The gas porosity is generally spherical and has a very fine dimension compared to other porosities [9]. Anton [3] believed that the low solubility of a gas in Ni-based superalloys and the vacuum melting could minimize the formation of gas porosities. The S-type forms at the final stage of solidification in the interdendritic regions [9, 10]. The H-type grows during solution heat treatment and forms due to the diffusion of vacancies during homogenization. The D-type forms by creep deformation with the diffusion mechanism [11]. The S-type porosities are mainly located at the interdendritic areas, so there is a relationship between the dendrite arm spacing and porosity distribution. It is well known that the formation of porosity mainly depends on the thermal gradient, withdrawal rate, and shrinkage factor of the alloy. Actually, Bachalet [12] proposed that there might be an optimum withdrawal rate for a certain alloy and casting, which resulted in the closely spaced dendrite arms and a minimum level of porosity. For example, an optimum withdrawal rate of 3–6 $mm.min^{-1}$ was found in directional solidified columnar castings of Mar-M247 alloy [13]. For a third-generation Ni-based single crystal superalloy an optimized withdrawal rate was found as about 7.5 $mm.min^{-1}$.
Although a great deal of research has been done on the relation between withdrawal rate and dendritic microstructure of directional solidified and single crystal superalloys [14-17], but there were few studies on the influence of withdrawal rate on the solidification microstructures and stress rupture properties for the Rene 80 superalloy. Therefore, the purpose of this paper was to investigate the effects of the withdrawal rate on the dendrite microstructure, the porosity, and the interaction between them. Furthermore, the formation mechanism of the dendritic structure was also discussed, and the stress rupture life of the alloy was determined.

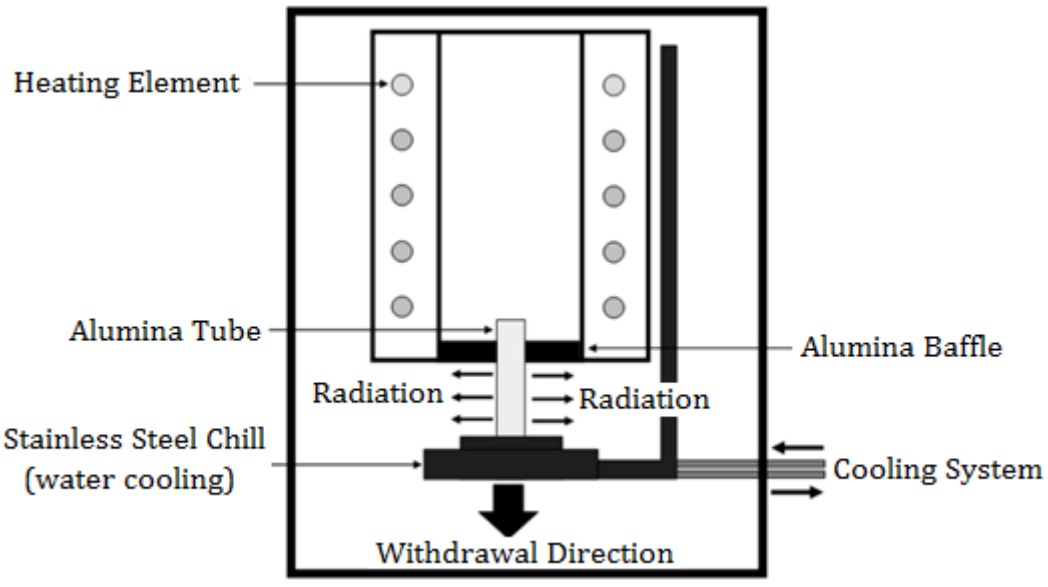

Fig. 1. Schematic representation of crystal growth system.

2. Experimental

Directionally solidified (DS) rods of Rene 80 superalloy with the standard composition 14Cr–9.5Co–5Ti–3Al–4W–4Mo–0.16C–0.015B–0.03Zr (wt.%) were prepared from 15 mm dia. cast ingots as a raw material. For this purpose, the raw material was melted and cast into five cylindrical ceramic tubes of 15 mm dia. and 140 mm height using vacuum induction melting (VIM) furnace. The furnace was evacuated to 10-3 Pa and purged with high-purity Argon. The temperature of the VIM furnace is controlled by adjusting the electric current and

power. The power of the furnace is 75 KW. These polycrystalline rods were directionally solidified in alumina tubes with the mentioned dimensions using a Bridgman crystal growth system with water-cooled steel chills. A schematic of the system is shown in Figure 1. The method involves heating polycrystalline above its melting point and slowly cooling it from one end where a steel-cooled chill crystal is located. The withdrawal rates of the directional solidification process were selected over a wide range, i.e., R=2, 4, 6, 8, and 10 mm.min^{-1}. The superheating temperature of the process was 1550˚C.

Metallographic sections were prepared using standard polishing procedures according to ASTM E3-01. The microstructure was revealed using a Marble solution. A VEGA TESCAN scanning electron microscope (SEM) with an energy dispersive spectroscopy (EDS) analyzer operating at 15KV and Olympus optical microscope (OM) were used to analyze the morphology and distribution of the phases. In addition, the Image J software was used to quantify and analyze the microstructure and measurement of primary dendritic arm spacing (PDAS) and secondary dendritic arm spacing (SDAS). The heat treatment schedule of Rene 80, according to the general procedure is consisted of 1024°C-2h (FC) + 1093°C-4h (FC) +1054°C-4h (FC), followed by aging at 873°C for16 h (AC). The cycles are drawn in Figure 2. The stress-rupture tests were carried out at 191 MPa and 980°C. The test was conducted according to ASTM E139. Schematic of the stress-rupture specimens is shown in Figure 2.

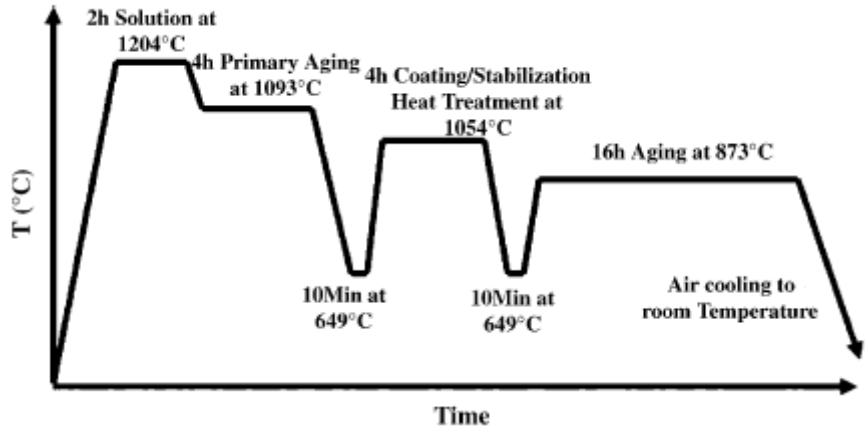

Fig. 2. Schematic of the heat treatment cycles of Rene 80 superalloy according to general electric standard.

3. Results and Discussion

3.1. Dendritic structure

Microstructural analysis of as-cast DS alloys under various withdrawal rates showed that up to the height of 20 mm from the chill plate, the melting was not completely achieved, and the alloy structure was not columnar (see Figure 3). This could be due to the high-temperature gradient in this zone as well as the inappropriate function of the baffle in this zone. As a result, the dendritic structure of the alloy was evaluated in three heights of 40, 60, and 80 mm of directionally solidified cylinder.

Based on the models presented for directionally solidified alloys growth including Hunt [18], Kurz-Fisher [19], and Trivedi [20], the relationship between PDAS and the growth rate of the solidification front (withdrawal rate) can be defined by Eq. 1. Kattamis and Flemings [21] also mentioned the relation between SDAS and growth rate as Eq. 2. The presented models deal with binary alloys. Therefore, due to the complexity of the chemical composition of DS superalloys, it is difficult to precisely predict the microstructure resulting from different solidification rates.

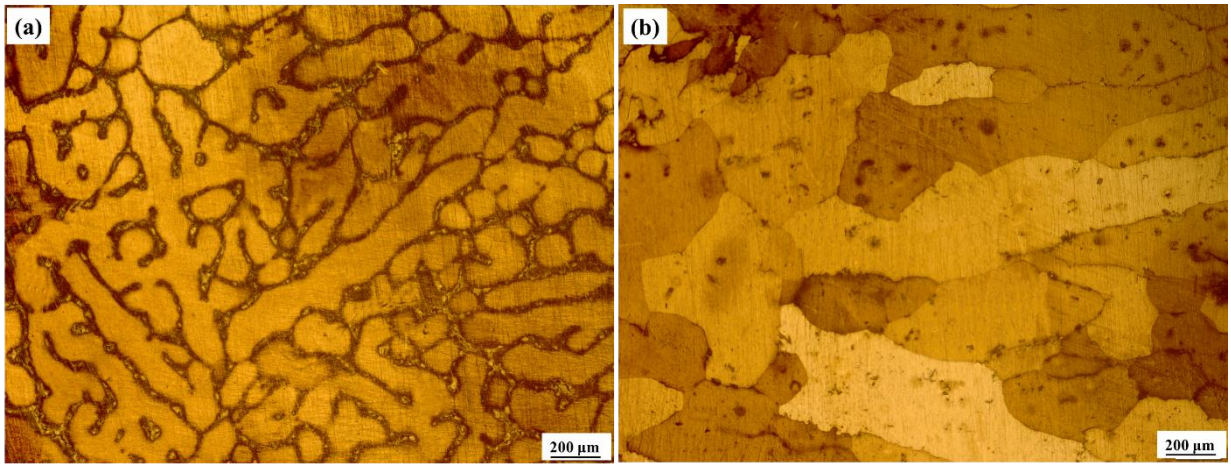

Fig. 3. Microstructure of the DS rods at the height 20 mm from the sill plate under withdrawal rates (a) 2 mm.min^{-1} and (b) 10 mm.min^{-1}.

(1) $\text{PDAS} \propto \text{R}^{-0.25}G^{-0.5}$ [18-20]

(2) $\text{SDAS} \propto \text{R}^{-\frac{1}{3}}$ [21]

Figures 4 and 5 show the longitude and transverse sections of dendritic structures of the directionally solidified specimens at the height of 60 mm. Moreover, the PDAS and SDAS as a function of withdrawal rate (R) and distance from the chill are depicted in Figure 6. As can be seen, an increase in withdrawal rate from 2 to 10 mm.min^{-1} resulted in a decrease of primary (PDAS) and secondary dendrite arm spacing (SDAS) from 293 and 89 m to 232 and 44 m, respectively. The results are compatible with Eq. 1 and 2, as with increasing withdrawal rate as well as increasing solidification rate, a finer dendritic structure was formed. Therefore, a reduction of PDAS and SDAS at high rates is expectable.

In all the specimens, by getting farther from the chill plate, PDAS showed an increase which may be attributed to temperature gradient loss in these zones [22]. An increase in the withdrawal rate caused to increase in the undercooling and which limits the growth of dendritic structure; hence, SDAS declined, similar to PDAS. Therefore, it is possible to change the solidification behavior of the alloys and hence alternate the slope of PDAS curve as a function of R. It seems that an increase in withdrawal rate will decrease the temperature gradient in the melted substance. Moreover, by getting farther from the chill plate, SDAS values increased, which may be attributed to the effect of temperature gradient decline in distances far away from the chill plate [22]. Therefore, the solidification time was increased, and primary and secondary dendrite arms will have a longer time for growth.

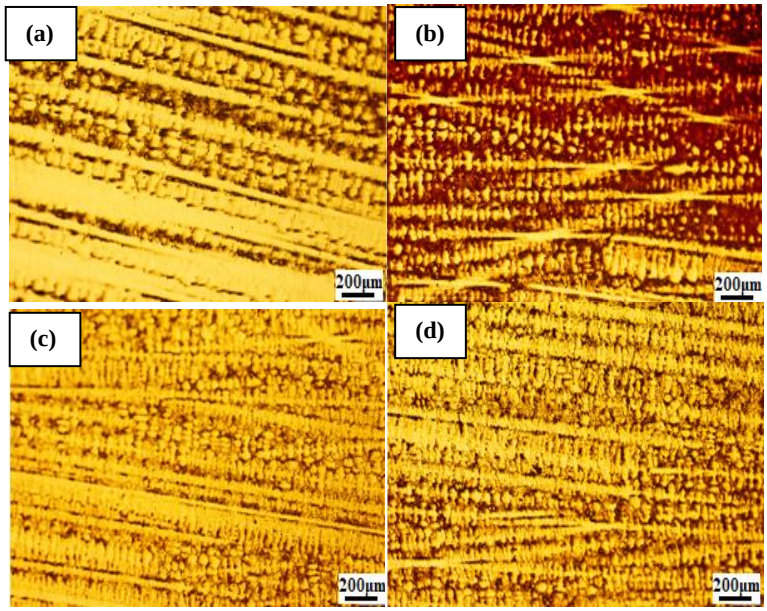

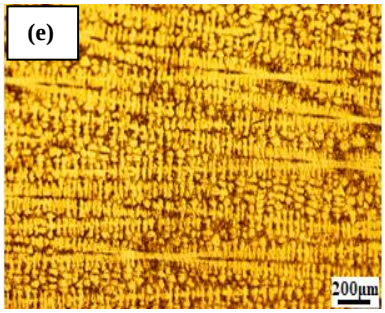

Fig. 4. Longitudinal sections of DS Rene80 rods at the height of 60 mm that directionally solidified under withdrawal rate of (a) 2; (b) 4; (c) 6; (d) 8 and (e) 10 mm.min^{-1}.

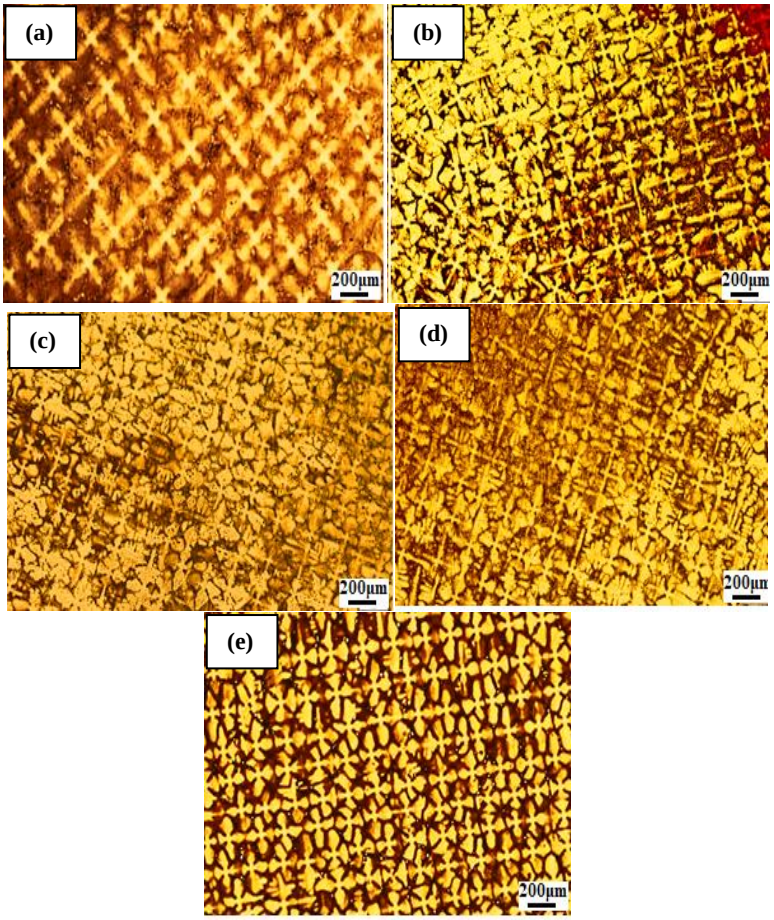

Fig. 5. Transverse sections of DS Rene80 rods at the height of 60 mm that directionally solidified under withdrawal rate of (a) 2; (b) 4; (c) 6; (d) 8 and (e) 10 mm.min^{-1}.

3.2. Microporosities

In the present study, microporosity refers to solidification porosity or S-type porosity formed as the result of the contraction of the final melt in interdendritic zones. Gas porosities are also possible. The probability of this type of porosity is low due to vacuum solidification. The distribution of the microporosities was evaluated by the graphs obtained at three heights of 40, 60, and 80 mm. Figure 7a and b represent the optical images of porosity distribution in DS specimens solidified at withdrawal rates of 2 and 10 mm.min^{-1}, respectively. One can see that, with an increasing solidification rate, a finer distribution of microporosities has been attained.

Figure 7c shows an S-type porosity in the vicinity of a eutectic island. It seems that the obtained porosity was formed in the last stage of solidification due to trapping and lack of melt feeding in this zone. Figure 8 illustrates the size, volume fraction, and number of porosities in terms of withdrawal rate. The porosities are quantified according to the E2109 ASTM standard. It was observed that an increase in withdrawal rate from 2 to 10 mm.min^{-1} decreased the size of microporosities from 13.2 to 8.7 µm.

Decreasing the dendritic arm spacing as a result of the withdrawal rate increasing causes to decrease in the pore's growth rate and hence declines their size. On the other hand, an increase of the withdrawal rate from 2 to 10 mm.min^{-1} increased the number of pores per section from 128 to 271. With the increase of the withdrawal rate and finer dendritic structure, the number of porosity germination sites increased. The major reason for the emergence of contraction microporosities is improper melt feeding in interdendritic regions. Therefore, when the dendritic structure gets finer, and the number of dendrites increases, the number of potential regions for contraction porosities formation will increase. On the other hand, enhancing the withdrawal rate from 2 to 6 mm.min^{-1} decreased the porosity from 0.26% to 0.15%. Further increase of withdrawal rate from 6 to 10 mm.min^{-1}, however increased the porosity percentage from 0.15% to 0.24%. Therefore, it can be said that the rate of 6 mm.min^{-1} is the optimum rate giving rise to the lowest porosity percentage in the as-cast structure. As it can be seen in Figure 9, there is a direct relationship between these parameters: finer dendritic structures will have smaller pores.

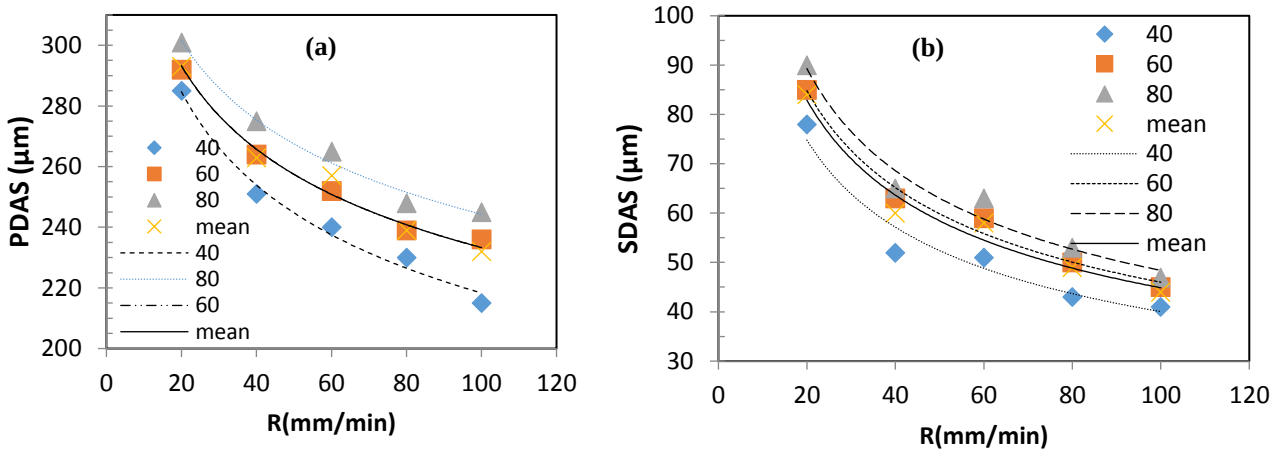

Fig. 6. (a) PDAS and (b) SDAS with withdrawal rate at different distances from the chill plate.

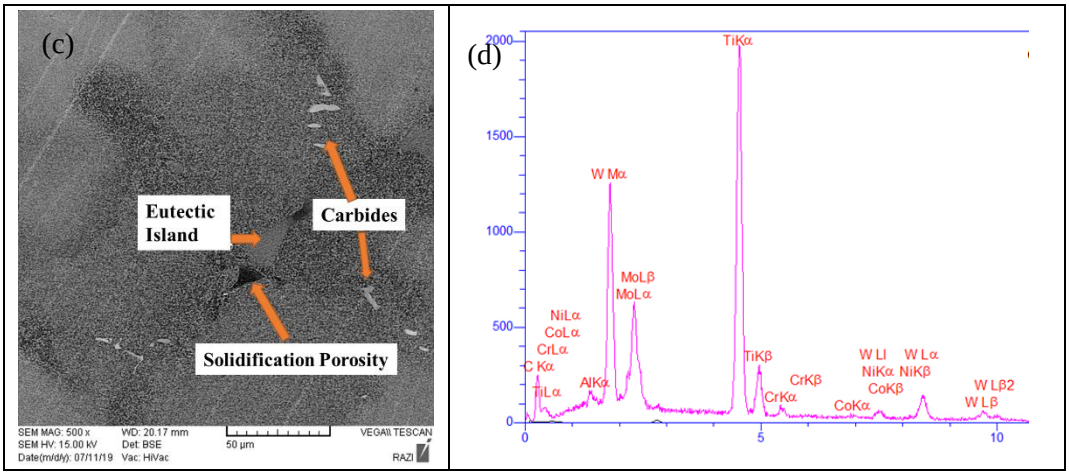

Fig. 7. Microporosities in DS Rene 80 rods that directionally solidified under withdrawal rates of (a) 2; (b) 10 mm.min^{-1}, and (c) the solidification microporosity at the adjacent of eutectic phase at 2 mm.min^{-1} and (d) EDS analysis of Carbide phase.

3.3. Eutectic Islands

Figure 9a and b show an optical image of eutectic islands in the specimens solidifies at 2 and 10 mm.min^{-1}, respectively. It can be seen that the eutectic structure is dependent on the dendritic structure. Due to the thermal gradient drop at 10 mm.min^{-1} growth rate, tertiary dendrite arms have been grown from the secondary ones. Therefore, a continuous network of the eutectic structure has been generated. As it is shown in Figure 10, with increasing withdrawal rate from 2 to 8 mm.min^{-1}, the eutectic volume percent has been decreased, while at 10 mm.min^{-1}, the eutectic volume percent has increased.

Figure 9c show the SEM image of a eutectic island in the specimen solidified at 8 mm.min^{-1}. This zone highly resembles the shape of a footprint; in a way that coarse γ' is like foot fingers, and fine ones along with γ' phase was also created while both sections are linked to a dendrite. Warnken [23] named them as

fan-like and checkerboard-like sections, respectively. There is a controversy on the formation of these structures. Early research proposed that fan-like structures were first formed, and then fine checkerboard-like structures were formed from the melt [24]. This is rarely possible as it requires ultrahigh supercooling and numerous nucleation sites in the final melt. Regarding the nature of γ′nucleation in the solid phase, the hypothesis of the primary formation of checkerboard-like sections with high nucleation sites and then the emergence of fan-like regions from the final melt sounds more rational [25]. On the other hand, as one can see in Figure 9c, even in the checkerboard-like section (fine), eutectic islands with distinct boundaries were formed. Hence, it seems that the mechanism of checkerboard-like section formation is something between the formation of γ' precipitates in the solid phase (ordering) and melt-to-solid eutectic transformation.

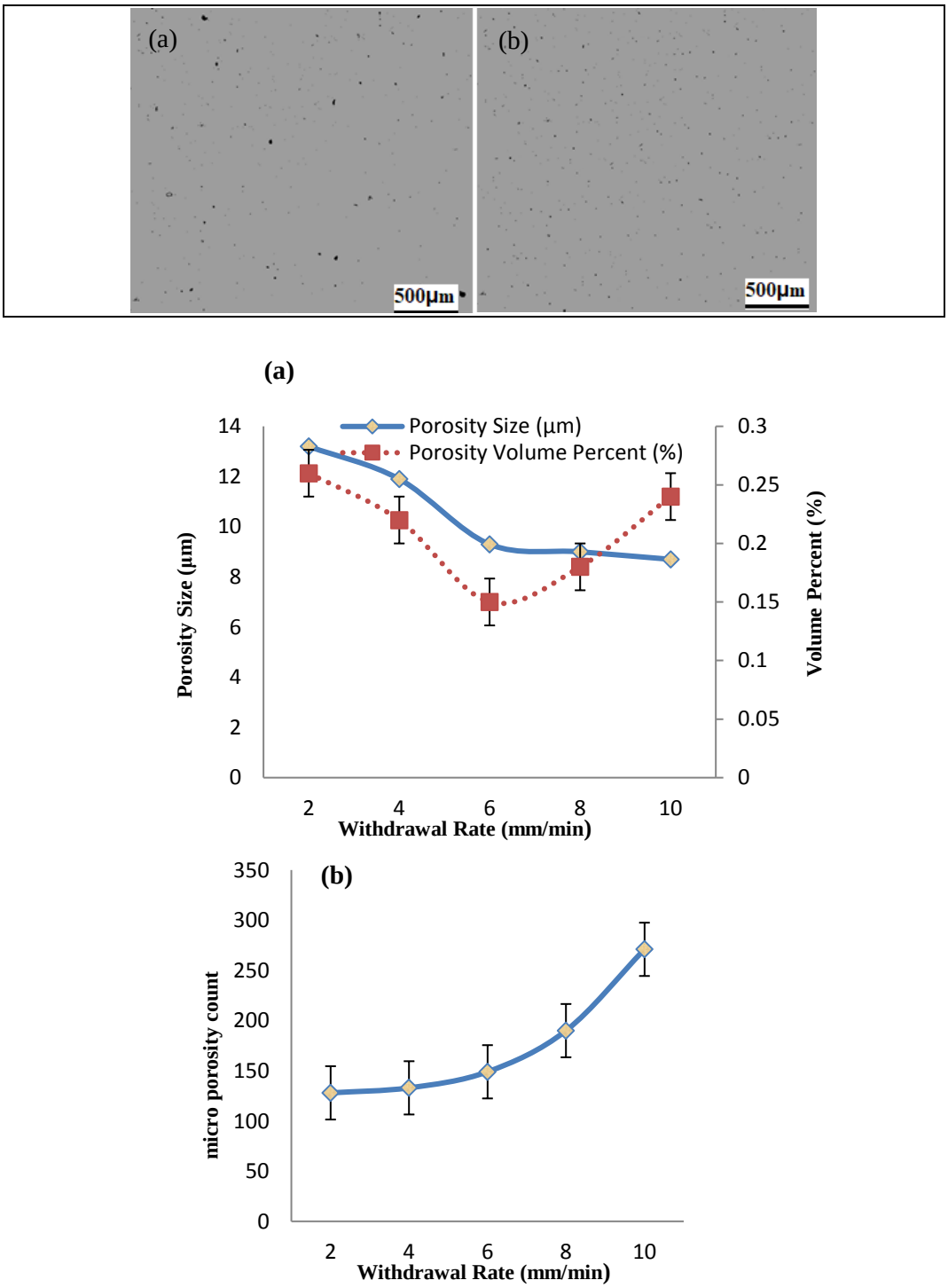

Fig. 8. (a) The size and volume percent of micro-porosities, and (b) micro-porosities number per section.

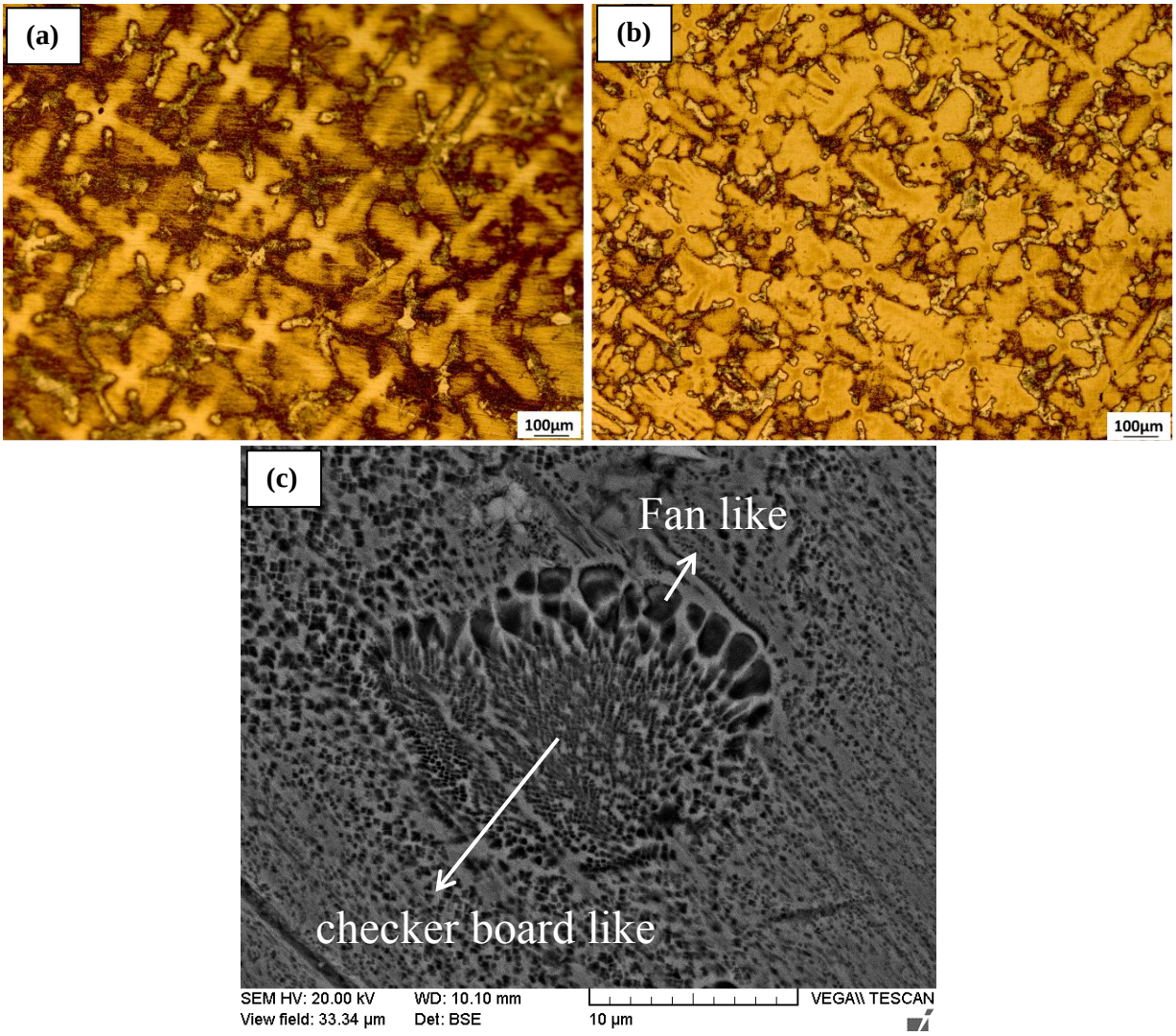

Fig. 9. Optical image of eutectic islands in the specimens solidified at (a) 2, (b) 10 mm.min^{-1}, and (c) SEM micrograph of the checkerboard-like and fan-like structure of eutectic phase for DS Rene 80 solidified at 8 mm.min^{-1} withdrawal rate.

Ordering, peritectic and eutectic transformations of Ni-based superalloys are expressed in equations 3 to 5.

$\gamma \rightarrow \gamma + \gamma'$ ordering (3) [26]

$L + \gamma \rightarrow \gamma'$ peritectic (4) [26]

$L \rightarrow \gamma + \gamma'$ eutectic (5) [26]

Ordering transformation completely occurs through solid-state diffusion, while peritectic transformation involves diffusion in both melted and solid phases. On the other hand, eutectic transformation only considers diffusion in the melt state [26]. Moreover, based on Eq. 6 [27], the melt diffusion coefficient (D_l) is far higher than its counterpart in the solid state (D_s). Therefore, it seems that the growth kinetics of eutectic transformation is higher than the peritectic one. So, it can be expressed that in the eutectic island, fine Checker Board-like sections are formed by peritectic transformation while the eutectic transition is responsible for the formation of fan-like structure in the last stage of solidification.

$D_l \gg D_s$ (6) [27]

3.4. Stress rupture strength

Stress-rupture tests were carried out at 191 MPa, and 980°C on the specimens, and the results are shown in Figure 11. The sample with less solidification microporosity and well-orientated dendritic structure, i.e., the one directionally solidified at 6 mm.min^{-1} gives higher rupture life of 25.43 hrs. Figure 8a shows that the samples solidified at the rate of 6 mm.min^{-1} has the least volume fraction of porosity, and also these porosities have the least size. At the withdrawal rate of 8 and 10 mm.min^{-1}, the rupture life decrease to 10 and 12 hrs, respectively. These two samples have the most volume fraction of microporosity that could reduce the rupture life. Nakagava et al. [28] tested the tensile and stress rupture properties of Rene 80, which directionally solidified at 3 and 6 mm.min^{-1}. They found that the best tensile strength at 870°C is for the withdrawal

rate of 3 mm.min^{-1}. They also reached the rupture life of 44.3 hrs at 190 MPa and 982°C for the sample, which directionally solidified at the withdrawal rate of 6 mm.min^{-1} [28]. For DD10 superalloy, the maximum rupture life of 79.8 hrs at 235 MPa and 1000°C was found at the withdrawal rate of 12 mm.min^{-1} [19]. Furthermore, these two samples have freckle defects that will be discussed in another paper.

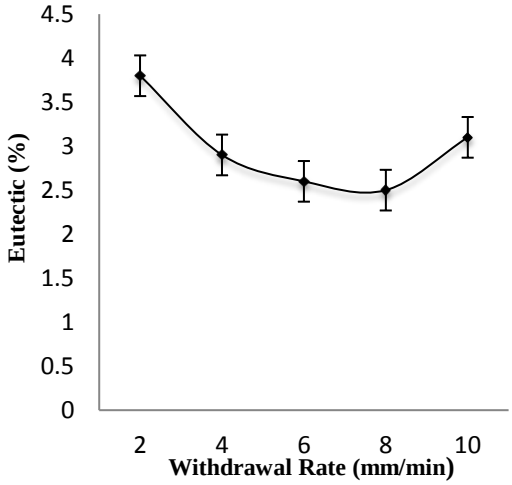

Fig. 10. The volume percent of eutectic with withdrawal rate.

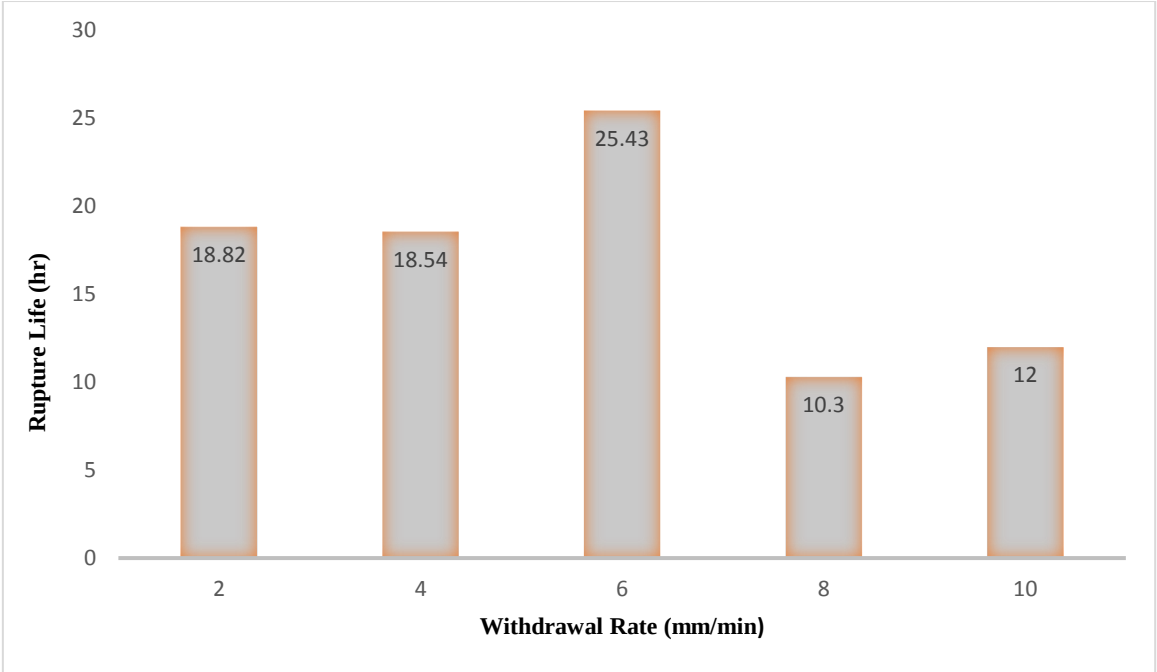

Fig. 11. Variation of stress rupture life as a function of withdrawal rate.

4. Conclusions

Based on the findings of the present study, the following conclusions are drawn:

(1) The relationships between withdrawal rate and dendrite arm spacings were investigated, and it was found that withdrawal rate has a direct effect on PDAS and SDAS.

(2) Increase of withdrawal rate from 2 to 10 mm.min^{-1} reduced the microporosity size from 13.2 to 8.7 µm. By increasing of withdrawal rate, the microporosity volume fraction decreased to 0.15 Vol% at 6 mm.min^{-1} and increased to 0.24 Vol% at 10 mm.min^{-1}. This is due to the increase of nucleation site of pores as the result of finer dendritic structure. Therefore, a withdrawal rate of 6 mm.min^{-1} is the optimal value to obtain a structure with minimum porosity and proper mechanical features.

(3) In the eutectic island, fine Checker Board-like sections are formed by peritectic transition, while the eutectic transition is responsible for the formation of a fan-like structure in the last stages of solidification.

(4) The sample directionally solidified at 6 mm.min^{-1} with less solidification microporosity and well-

orientated dendritic structure gives higher rupture life of 25.43 hrs.

References

[1] R. C. Reed. The superalloys: fundamentals and applications. Cambridge: Cambridge university press; 2008.
[2] C. Yang, Y. Xu, H. Nie, "Effects of heat treatments on the microstructure and mechanical properties of Rene 80", Mater. Des., Vol. 43, 2013, pp. 66–73.
[3] A. Ohtomo, Y. Saiga, "Directional solidification of Rene' 80", Jpn. Inst. Met. Trans., Vol 17, 1976, pp 323–329.
[4] H. Zhang, O. A. Ojo. J. Mater. Sci. "TEM analysis of Cr–Mo–W–B phase in a DS nickel based superalloy", Vol. 43, 2008, pp. 6024–6028.
[5] T. Goswami, H. Hänninen, "Dwell effects on high temperature fatigue behavior –. Part I.", Mater. Des., Vol.22, 2001, pp. 199–215.
[6] R. K. Sidhu, O. A. Ojo, M. C. Chaturvedi, "Sub-solidus melting of directionally solidified Rene 80 superalloy during solution heat treatment", J. Mater. Sci., Vol. 43, 2008, pp. 3612–3617.
[7] A. Szczotok, B. Chmiela, "Effect of Heat Treatment on Chemical Segregation in CMSX-4 Nickel-Base Superalloy", J. Mater. Eng. Perform., Vol. 23, 2014, pp. 2739–2747.
[8] L. Kunz, P. Lukáš, R. Konečná, "Casting defects and high temperature fatigue life of IN713LC superalloy", Int. J. Fatigue., Vol. 41, 2012, pp. 47–51.
[9] Q. Yue, L. Liu, W. Yang, "Influence of withdrawal rate on the porosity in a third generation Ni based superalloy", Prog. Nat. Sci.: Mater. Int., Vol. 61, 2017, pp. 236–243.
[10] B. S. Bokstein, A. I. Epishin, T. Link, "Model for the porosity growth in single crystal nickel base superalloys during homogenization", Scr. Mater., Vol. 57, 2007, pp. 801–804.
[11] T. Link, S. Zabler, A. Epishin , "Synchrotron tomography of porosity in single crystal nickel base superalloys", Mater. Sci. Eng., Vol. 425A, 2006, pp. 47–54.
[12] E. Bachelet, G. Lesoult, "Quality of castings of superalloys. In: High Temperature Alloys for Gas Turbines", Liege, Belgium, 1978, pp. 665-699.
[13] S. Roskosz, M. Staszewski, A. Cwajna. "A complex procedure for describing porosity in precision cast elements of aircraft engines made of MAR-M 247 and MAR-M 509 superalloys", J. Mater. charact., Vol. 56, 2006, pp.405–413.
[14] J. Zhang, J. Li, T. Jin, "Effect of solidification parameters on the microstructure and creep property of a single crystal Ni base superalloy", J. Mater., Vol. 26, 2010, pp. 889–895.
[15] G. Sifeng , L. Lin , X. Yiku , "Influence of processing parameters on microstructure during investment casting of nickel base single crystal superalloy DD3", China Foundry, Vol. 9, 2012, pp.159–164.
[16] M. M. Zou, J. Zhang, J. G. Li, "Effect of melt overheating history on the microstructure of Ni-Base single crystal superalloy", Adv. Mater. Res., Vol, 217, 2011, 692–696.
[17] G. Liu, L. Liu, C. Ai, "Influence of withdrawal rate on the microstructure of Ni-base single-crystal superalloys containing Re and Ru", J. Alloys Compd., Vol. 509, 2011, pp. 5866–5872.
[18] J. D. Hunt, "Cellular and primary dendrite spacing. In: Solidification and Casting of Metals", Sheffield, England, 1977, pp. 3-9.
[19] W. Kurz, D. J. Fisher, "Dendrite growth at the limit of stability", Acta Metall., Vol 29, 1981, pp. 11–20.
[20] R. Trivedi, "Interdendritic spacing: Part II. A comparison of theory and experiment", Metall. Mater. Trans., Vol. 15A, 1984, pp. 977–982.
[21] T. Z. Kattamis, M. C. Flemings, " Dendrite morphology, micro-segregation, and homogenization of low-alloy steel", Transactions of the Metallurgical Society of AIME, Vol 233,1965, pp. 992-999.
[22] L. G. Peterson, "Directional solidification of land based gas. In: ASME 1989 International Gas Turbine and Aeroengine Congress and Exposition" American Society of Mechanical Engineers. 1989, pp. 332-337.
[23] N. Warnken N, "Studies on the solidification path of single crystal superalloys", J. Phase Equilib. Diffus., Vol. 37, 2016, pp.100–107.
[24] N. D'souza, H. B., Dong, "Solidification path in third-generation Ni-based superalloys with an emphasis on last stage solidification", Scr. Mater., Vol 56, 2007, pp. 41–44.
[25] A. Heckl, R. Rettig, S. Cenanovic, "Investigation of the final stages of solidification and eutectic phase formation in Re and Ru containing nickel-base superalloys" J. Cryst. Growth., Vol. 312, 2010, pp.2137–2144.
[26] Porter DA, Easterling KE, Sherif M. "Phase Transformations in Metals and Alloys". United States: CRC press; 2009.
[27] P. Shewmon, "Diffusion in solids", Springer, 2016.
[28] Y. G. Nakagava, A. Ohtomo and Y. Saiga, "Directional solidification of Rene 80", Trans. Japan Institute Met., Vol. 17, pp. 323-329, 1976.